THE JOURNAL OF BIOLOGICAL CHEMISTRY Vol. 277, No. 34, Issue of August 23, pp. 31005–31013, 2002
Printed in U.S.A.

Characterization of Regions in hsMAD1 Needed for Binding hsMAD2

A POLYMORPHIC CHANGE IN AN hsMAD1 LEUCINE ZIPPER AFFECTS MAD1-MAD2 INTERACTION AND SPINDLE CHECKPOINT FUNCTION*

Received for publication, November 6, 2001, and in revised form, April 17, 2002
Published, JBC Papers in Press, May 31, 2002, DOI 10.1074/jbc.M110666200

Yoichi Iwanaga, Takefumi Kasai, Karen Kibler, and Kuan-Teh Jeang‡

From the Molecular Virology Section, Laboratory of Molecular Microbiology, NIAID, National Institutes of Health, Bethesda, Maryland 20892-0460

In eukaryotes, the mitotic spindle assembly checkpoint provides a monitor for the fidelity of chromosomal segregation. In this context, the mitotic arrest deficiency protein 2 (MAD2) censors chromosomal mis-segregation by monitoring microtubule attachment/tension, a role that requires its attachment to kinetochores. Studies in yeast have shown that binding of MAD1 to MAD2 is important for the checkpoint function of the latter. The interactions between human MAD1 (hsMAD1) and human MAD2 (hsMAD2) have, however, remained poorly characterized. Here we report that two leucine zipper domains (amino acids 501–522 and 557–571) in hsMAD1 are required for its contact with hsMAD2. Interestingly, in several cancer cell lines, we noted the frequent presence of a coding single nucleotide Arg to His polymorphism at codon 558 located within the second leucine zipper of hsMAD1. We found that hsMAD1H558 is less proficient than hsMAD1R558 in binding hsMAD2 and in enforcing mitotic arrest. We also document a first example of loss-of-heterozygosity for a spindle checkpoint gene (at the *hsMAD1 558* locus) in a human breast cancer. Based on our findings, it is possible that hsMAD1H558 could be an at-risk polymorphism that contributes to attenuated spindle checkpoint function in human cells.

To maintain genome integrity, precise partitioning of chromosomes from one mother cell to two daughter cells occurs during mitosis. If spindle damage or segregation mistakes happen, a mitotic metaphase-to-anaphase checkpoint that halts propagation of error is activated (1, 2). Accordingly, cells arrest in metaphase until corrections are achieved and impartial allocation of chromosomes can be ensured. Loss of spindle checkpoint is one of several processes that could result in aneuploidy. Because deviation from euploidy is seen in 70–80% of all types of human cancers (3), aneuploidy could be an important contributor to transformation.

Genetics studies in yeast and mammals have implicated at least 7 genes (4, 5) in mitotic spindle checkpoint (MSC)[1] function, BUB (budding uninhibited by benomyl) 1–3 and MAD (mitotic arrest deficiency) 1–3, and Mps1 (monopolar spindle; see Refs. 6 and 7). The MAD BUB, and Mps1 proteins form complexes that regulate orderly chromosomal segregation and nuclear division (1, 2). Although details of how this complex works remain to be fully understood, it is generally agreed that the distal effector protein of the metaphase-anaphase checkpoint is MAD2, which has been found to bind CDC20 and to inhibit the function of the anaphase-promoting complex (8–10).

The high frequency of aneuploidy in cancers has prompted the thought that loss-of-function mutations in human BUB/MAD proteins might occur rather commonly. Intriguingly, empirical data have largely been incongruent with this hypothesis (11). Indeed, in a survey of 21 lung cancer cell lines and 25 primary lung cancers, Takahashi *et al.* (12) concluded there was a lack of any obviously inactivating mutation in hsMAD2. Similarly, Cahill *et al.* (13) found only limited changes in BUB1 from a series of 19 colorectal cancers (*i.e.* two total changes, a single missense mutation, and a 197-bp internal deletion). Currently a definition of simple recessive mutation(s) that prevalently explains aneuploidy remains elusive.

Mechanistically, binding of the spindle effector protein, hsMAD2, to kinetochores is a critical step in mitotic checkpoint function. During mitosis, unattached kinetochores attract MAD2 to produce a diffusible "wait anaphase" signal (14, 15) which is then silenced by spindle attachment. We previously identified and cloned an intracellular binding partner of hsMAD2, human MAD1 (16), whose intracellular biological activity remains largely uncharacterized. Earlier it was thought that oligomerized hsMAD2 was wholly sufficient to produce cell cycle arrest; however, recent data (17) suggest that binding of hsMAD2 to hsMAD1 rather than oligomerization is the critical step required for spindle checkpoint function. Because *Mad2* mutations in aneuploid tumors are exceedingly rare (12, 18, 19) and because binding of MAD2 to MAD1 is required for checkpoint function (17), we wondered whether frequent loss of MAD2-associated wait anaphase function might be because of changes in its binding protein, MAD1. Here we show that human MAD1 dominantly dictates MAD2 migration into kinetochore-proximal nuclear punctates through a process that requires MAD1-MAD2 binding. We also show that binding of full-length MAD2 by full MAD1 requires two leucine zipper domains (amino acids 501–522 and 557–571) in hsMAD1. One of these two leucine zipper domains is disrupted by an Arg-558 to His-coding single nucleotide polymorphism in *mad1* allele frequently found in many human cancer cell lines.

EXPERIMENTAL PROCEDURES

Cells and Plasmids—HeLa and Hct116 cells were cultured in Dulbecco's modified Eagle's medium/high glucose supplemented with anti-

* The costs of publication of this article were defrayed in part by the payment of page charges. This article must therefore be hereby marked "*advertisement*" in accordance with 18 U.S.C. Section 1734 solely to indicate this fact.

‡ To whom correspondence should be addressed: Bldg. 4, Rm. 306, 9000 Rockville Pike, Bethesda, MD 20892-0460. Tel: 301-496-6680; Fax: 301-480-3686; E-mail: kj7e@nih.gov.

[1] The abbreviations used are: MSC, mitotic spindle checkpoint; MAD2, mitotic arrest deficiency protein 2; LOH, loss-of-heterozygosity; hsMAD1, human MAD1; RFP, red fluorescent protein; aa, amino acids; GFP, green fluorescent protein; HTLV, human T cell lymphotrophic virus; TRITC, tetramethylrhodamine isothiocyanate.

a)

nucleotide	amino acid	2 colon	5 kidney	2 lung	3 prostate	5 uterus	6 HTLV	total 23 cancers
88 t → a	30 G → G		1			1		2
238 a → g	80 R → G	2	1					3
663 c → t	221 H → H	1	2		2			5
847 c → t	283 L → L		1	1		1		3
1596 g → a	532 Q → Q	1				1		2
1673 g → a	558 R → H	**1**	**2**	**2**	**2**	**2**	**3**	**12**
1730 c → t	577 A → V		2				2	4
1859 a → g	620 E → G				1	1		2

b)

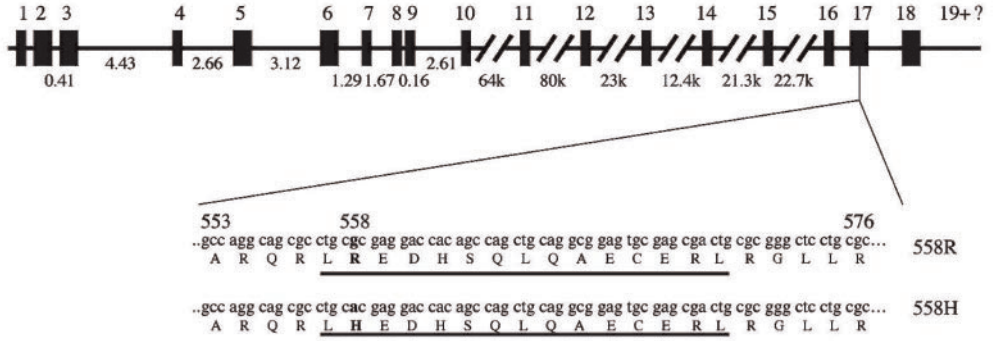

FIG. 1. **Frequent Arg to His (*R to H*) amino acid substitution at codon 558 in *hsMAD1* exon 17.** *a*, nucleotide and amino acid substitutions in cancers for *hsMAD1* coding sequences from 2 colon cancers, 5 kidney cancers, 2 lung cancers, 3 prostate cancers, 5 uterine cancers, and 6 HTLV-1 cells were examined. 4 conservative mutations and 4 missense mutations were found. Over 50% of the samples have a change at codon 558. *b*, a schematic diagram of the *hsMAD1* locus (27) on chromosome 7 is shown. *Black bars* indicate exons. The expanded portion shows the nucleotides and amino acids for exon 17. The arginine (*R*) to histidine (*H*) substitution at codon 558 is indicated. *Underlines* denote a leucine zipper domain that contains codon 558. *Bold lettering* indicates an *Acc*II restriction site in the Arg-558 allele; ***a*** shows the substituted nucleotide in His-558.

biotics (100 units/ml penicillin-G, 100 μg/ml streptomycin) and 10% fetal bovine serum. hsMAD1 expression vector was constructed by in-frame insertion of full-length MAD1 open reading frames with either 558R or 558H codon into pcDNA4HisMax vector (Invitrogen). Deletions in hsMAD1 and hsMAD2 were by PCR-based mutagenesis. All mutations were confirmed by sequencing. Fragments were inserted in-frame into pEGFP-C1 or pDs-Red-C1 vector (CLONTECH). Transient transfection of HeLa and Hct116 cells was performed using LipofectAMINE reagent (Invitrogen) according to the manufacturer's protocol.

Sequence and Mutational Analysis—Sequence information of hsMAD1 is based on NM003550 in which we corrected a 1-nucleotide-insertion sequencing error by us previously reported under GenBank™ accession number U33822. PCR amplification for *hsMAD1* cDNA or genomic DNA was performed with GC-RICH PCR system (Roche Molecular Biochemicals). The entire coding sequences of hsMAD1 were amplified from tumor cDNA libraries (matched cDNA pairs from tumor and normal tissues: CLONTECH) and cDNA generated by cells to cDNA (Ambion) from cancer cell lines, using the following primers 5′-ATATATGAATTCCATGGAAGACCTGGGGGAAAACACC-3′ and 5′-AAATTTGGATCCGATTTTATTTCACAAGGTGAGGAAC-3′, digested with *Eco*RI and *Bam*HI, and cloned into pUC vector for sequencing. *hsMAD1* exon17 was amplified from genomic DNA using the following primers: 5′-GTGTGAGAATTCCTGCAGGGTGACTATGACCAG-3′ and 5′-GAGTCTGGATCCCTGCCACCTCCTTGGACGATGGCAGAC-3′. Where indicated, genomic PCR products were also digested with *Acc*II for analysis.

Immunofluorescence and Confocal Microscopy—Asynchronous HeLa cells were fixed with methanol, stained with anti-hsMAD1 monospecific antibody and anti-kinetochore human serum ANA-C (Sigma), washed, and visualized by incubation with anti-mouse IgG fluorescein isothiocyanate (Sigma) and anti-human IgG TRITC (Sigma). HeLa cells transfected with GFP-hsMAD1 were fixed with methanol, stained with ANA-C, washed, and visualized by staining with anti-human IgG TRITC. Live HeLa cells transfected with GFP-hsMAD1, GFP-hsMAD2, or RFP-hsMAD2 were visualized by confocal microscopy Axiovert 135M (Carl Zeiss).

Co-immunoprecipitation and Western Blotting—HeLa cells transfected with pcDNA4/HisMax-558R or -558H were harvested 48 h after transfection. Cells were lysed in co-immunoprecipitation buffer (50 mM Tris, pH 7.5, 15 mM EDTA, 100 mM NaCl, 0.1% Triton X-100) with protease inhibitor mixture (Complete; Roche Molecular Biochemicals), and the extracts were immunoprecipitated with anti-Xpress (Invitrogen). Precipitates and whole cell lysates resolved in 12% SDS-PAGE were transferred to Immobilon-P membrane (Millipore). hsMAD1 and hsMAD2 proteins were detected with anti-HisG (Invitrogen) or anti-hsMAD2 antibody (Transduction Laboratories), respectively. Blots were visualized by chemiluminescence (Tropix). Whole cell lysates of KG1 or LS411N cells resolved in 10% SDS-PAGE were transferred to membrane and detected with anti-hsMAD1 antibody.

Mitotic Indices—Cells were cotransfected with EGFP-C1 plasmid and pcDNA4HisMax-558R or -558H or control plasmid. 24 h after transfection, cells were treated with 0.2 μg/ml nocodazole. Cells were fixed with 1% formaldehyde, 0.2% glutaraldehyde and stained with 10 μg/ml Hoechst 33258 (Sigma). To measure mitotic indices, at least 300 cells with green signal were counted per assay at the indicated times after nocodazole treatment. In Fig. 9, mitotic indices were measure in Hoechst 33258-stained cells without transfection.

RESULTS

A Frequent Single Nucleotide Polymorphism Affects hsMAD1 Function—The rarity of *Mad2* mutations in aneuploid human tumors led us to ask whether loss of *hsMad2*-dependent spindle checkpoint function might instead emanate from changes in *hsMad1*. To investigate this possibility, we surveyed human cancer cells for alterations in *Mad1*. We directly sequenced *Mad1* open reading frames from 17 solid tumors and 6 HTLV-1-transformed cells. From these 23 samples, several sporadic and inconsistent point changes in *Mad1* were noted (Fig. 1*a*). However, one frequent (>50% occurrence) and consistent finding was a change in exon 17 of *hsMad1*. Here, a coding single nucleotide g to a polymorphism at codon 558 (Fig. 1*b*) replacing an Arg (arginine) with an His (histidine) was found in 9 of 17 solid tumors and 3 of 6 HTLV-transformed cells.

Previously, Cahill and colleagues (13) had raised the example that a single amino acid substitution in BUB1 was sufficient to alter mitotic spindle checkpoint. Thus, we considered whether the Arg to His substitution at codon 558 in hsMAD1 might also influence function. MAD1 has a long coiled-coil structure that is highly conserved in *Drosophila*, *Xenopus*, rodents, and primates. Residue 558 lies within a leucine zipper region that was suggested to be important for the protein-protein binding of hsMAD1 (20).

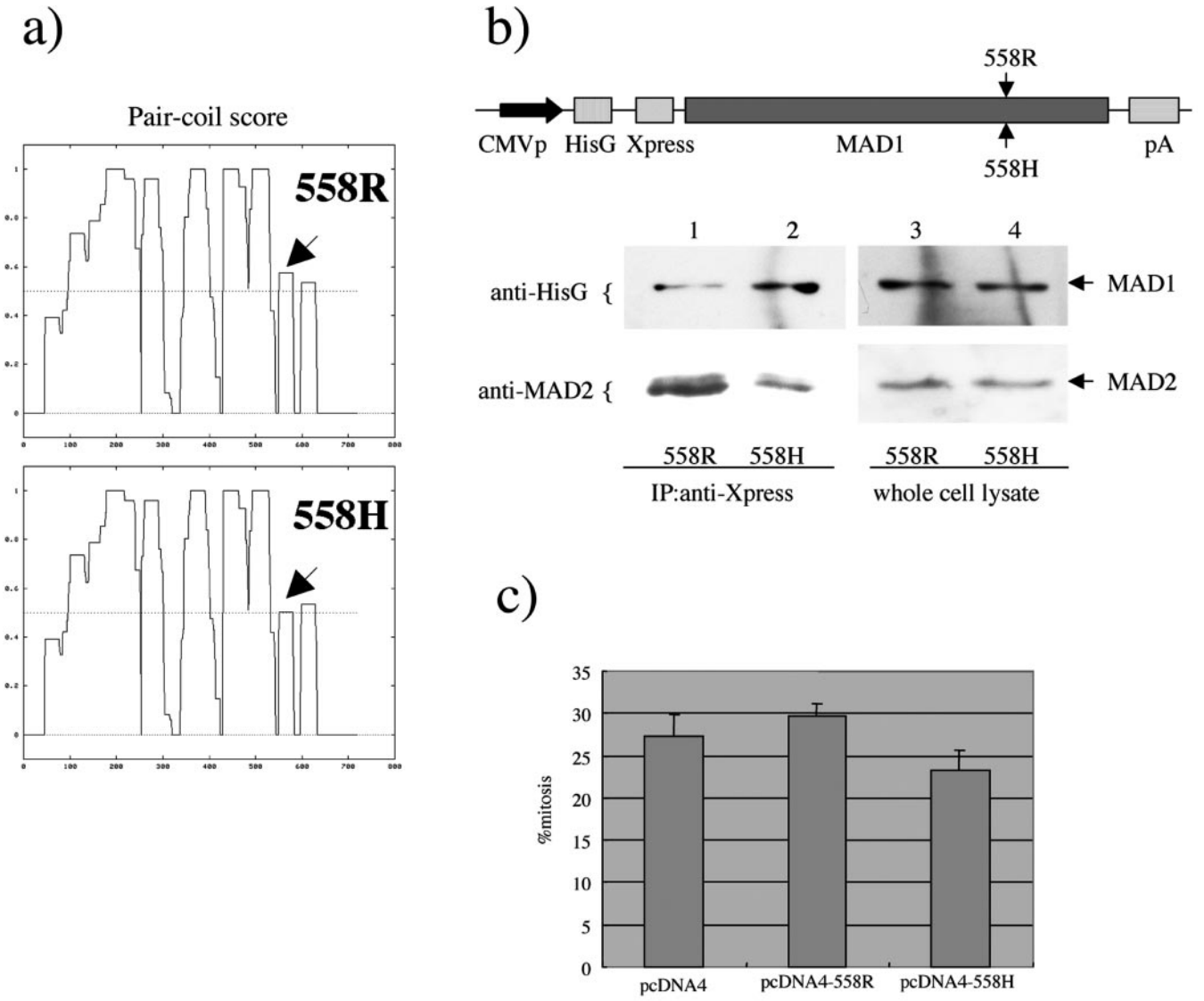

FIG. 2. **Loss of checkpoint activity of hsMAD1H558.** *a*, comparison of predicted coiled-coil structures between hsMAD1R558 and -H558. The *y* axis is the probability of forming coiled-coils. The plots were produced by the PAIR-COIL program with MTIDK matrix at the COILS website (www.ch.embnet.org/software/COLIS_form.html). *b*, schematic representation of hsMAD1 expression vectors based on pcDNA4 HisMax plasmid (*top*). Co-immunoprecipitation of hsMAD2 with either hsMAD1R558 or hsMAD1H558 was performed with HeLa cells transfected with either pcDNA4HisMax-558R (*lane 1*) or pcDNA4HisMax-558H (*lane 2*). Immunoprecipitation was with anti-Xpress. Western blottings were with anti-HisG or anti-MAD2. *c*, mitotic indices of Hct116 cells overexpressing either hsMAD1R558 or hsMAD1H558. Cells were co-transfected with a green fluorescent protein (*GFP*) expressing plasmid, pEGFP-C1 plus pcDNA4HisMax vector (*pcDNA4*), or pcDNA4HisMax-558R (*pcDNA4–558R*), or pcDNA4HisMax-558H (*pcDNA4–558H*). After 6 h of nocodazole treatment, GFP-positive cells were scored. Values are averages from three independent assays; *error bars* represent S.E.

Computer modeling implicates the Arg to His change at position 558 to produce a small but distinct perturbation in the coiled-coil of hsMAD1 (Fig. 2*a*). We wondered whether this might commensurately affect protein-protein binding between hsMAD1 and hsMAD2 (16) thereby disturbing MAD2-dependent function. We constructed two otherwise isogenic hsMAD1 expression vectors that respectively encoded for either MAD1R558 or MAD1H558. Both vectors were tagged identically at their N termini with consecutive HisG and Xpress epitopes (Fig. 2*b*). The two vectors were separately introduced into cells. Transfected cells were found to express equally the two exogenously introduced MAD1 proteins (Fig. 2*b*, *lanes 3* and *4*, *anti-HisG*) as well as to have equal amounts of cell endogenous MAD2 protein (Fig. 2*b*, *lanes 3* and *4*, *anti-MAD2*). We then immunoprecipitated whole cell lysates with anti-Xpress (Fig. 2*b*, *lanes 1* and *2*), and we measured the amount of immunoprecipitated Xpress-tagged MAD1 and co-precipitated MAD2 by Western blotting with anti-HisG (Fig. 2*b*, *lanes 1* and *2*, *top*) and anti-MAD2 (Fig. 2*b*, *lanes 1* and *2*, *bottom*), respectively. Normalizing for recoveries, we found that consistent with the predicted disturbance in coiled-coil sequence MAD1H558 was 4.5-fold worse than MAD1R558 in binding MAD2.

We next asked whether the MAD1R558 to MAD1H558 change influences intracellular mitotic checkpoint. To address this, we transiently transfected spindle checkpoint intact Hct116 cells separately with vectors expressing either MAD1R558 or MAD1H558. The transfected cells were then challenged with microtubule-disrupting agent, nocodazole, to induce checkpoint activity. Competency of mitotic arrest was assessed. To minimize the potential for cellular adaptation and resulting mitotic slippage (21), mitotic indices were monitored within 6 h of exposure to nocodazole. In this rapid single round cell cycle measurement, we consistently found MAD1H558 to reduce the efficiency of nocodazole-induced mitotic arrest (Fig. 2*c*) by 8–10% when compared with MAD1R558. Because only a

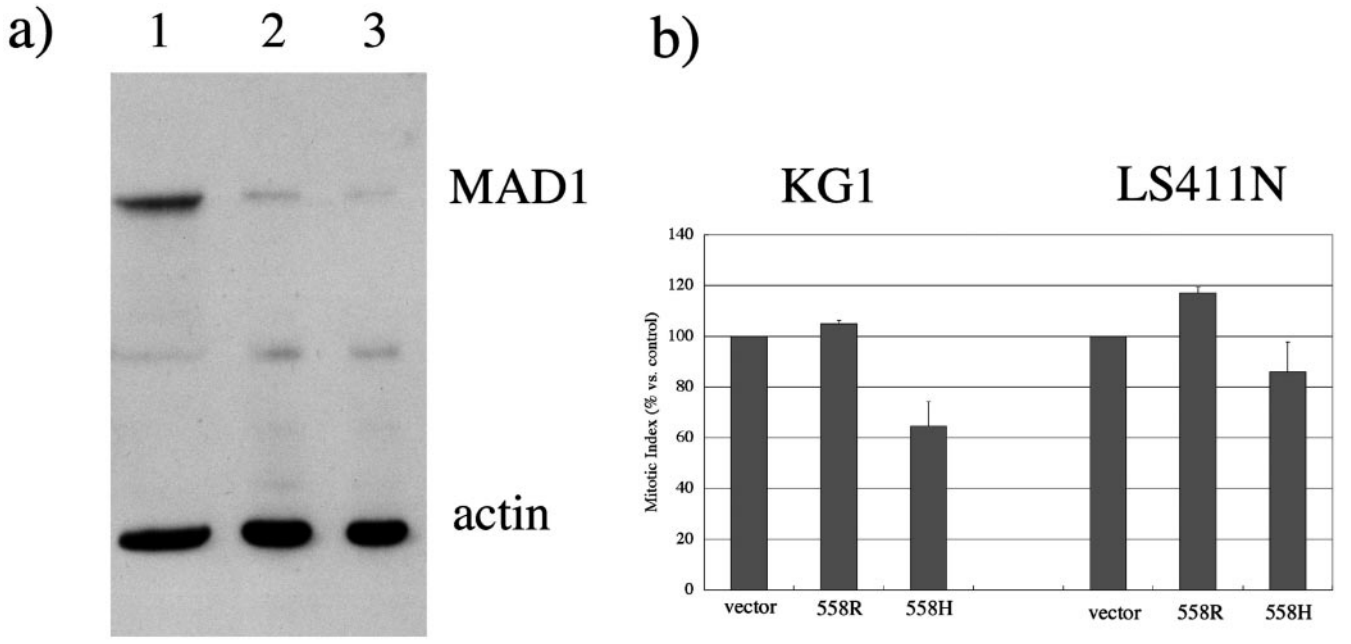

FIG. 3. **Dominant-negative effects of hsMAD1558H in cells haplotypic for *hsMad1*.** *a*, Western blotting analysis shows reduced amount of MAD1 in two human cell lines with monosomy 7 (*KG1, lane* 2; and *LS411N*, *lane 3*). Diploid Hct116 cells are shown in *lane 1*. The blot was probed with mono-specific anti-hsMAD1 serum as well as with monoclonal anti-β-actin antibody. The actin signals provide controls for equivalence of sample loading. *b*, mitotic indices of monosomy 7 cells overexpressing hsMAD1R558 or hsMAD1H558. Cells were co-transfected with pEGFP-C1 and pcDNA4HisMax vector (vector), or pcDNA4HisMax-558R (558R), or pcDNA4HisMax-558H (558H). After 6 h of nocodazole treatment, GFP-positive cells were scored. Values are averages from three independent assays; *error bars* represent S.E.

minority (~25%; see pcDNA4 values, Fig. 2*c*) of these asynchronously cultured cells was poised to enter metaphase during the 6-h assay, if this effect were translated to a homogeneous population of metaphase-synchronized cells then single-round mitotic arrest differences between MAD1H558 *versus* MAD1R558 would range between 32 and 40%.

Hct116 is a diploid human colon cancer that expresses large amounts of endogenous MAD1 protein (Fig. 3*a*, *lane 1*). Because of its high level of MAD1, the true potency of exogenously introduced MAD1H558 could be partially masked in Hct116. We had previously mapped *hsMad1* to human chromosome 7 (22). Because monosomy 7 (*i.e.* a *Mad1* haplotype) is rather common in several types of human cancers, we sought to verify whether in settings of reduced MAD1 expression (*e.g.* monosomy 7 cells) the mitotic arrest differences between MAD1H558 and MAD1R558 would be enhanced. In two cell lines KG-1 (Fig. 3*a*, *lane 2*), an acute myelogenous leukemia with monosomy 7, and LS411N (Fig. 3*a*, *lane 3*), a human Dukes' type B cecum carcinoma with monosomy 7, were directly verified to have low amounts of endogenous MAD1. In these two cells, we repeated the comparison between MAD1R558 and MAD1H558. Consistent with expectation and with the above Hct116 results, we observed arrest efficiency differences of 30–40% between MAD1H558 and MAD1R558 (Fig. 3*b*). These results suggest that an *hsMad1h558* genotype superimposed on an otherwise *hsMad1* haplotype (*i.e.* monosomy 7) potentially conveys a worse cancer prognosis than an *hsMad1* haplotype alone.

hsMAD1 Locates hsMAD2 into Nuclear Bodies—The above functional observations prompted us to consider how MAD1H558 might mechanistically influence intracellular spindle checkpoint function. Previously, *in vitro* results from *Xenopus* egg extracts have suggested that soluble Xmad1 might recruit Xmad2 to kinetochores (23). However, potential biological differences between meiotic *Xenopus* soluble egg extracts and mitotic human cells question whether convergent or divergent rules govern MAD1, MAD2, and kinetochore interaction in the latter setting (24). For example, whereas CENP-E is required in *Xenopus* egg extracts for Xmad2 attachment to and signaling from kinetochores (24), depletion of CENP-E in HeLa cells paradoxically conferred chronic hsMAD2 association to and signaling from human kinetochores (25). Further confusing the understanding of MAD1/MAD2 activity in human cells, several different immunostained profiles of hsMAD1 during various stages of the cell cycle have been reported (16, 26). To understand better the MAD1H558 phenotype, we created chimeric green fluorescent (GFP)-hsMAD1 to analyze protein localization as well as intracellular interactions between MAD1 and MAD2.

Asynchronously cultured HeLa cells were transfected with a plasmid vector expressing GFP-hsMAD1. Cells were then examined for green fluorescence and also immunostained with anti-kinetochore antibody, ANA-C (Fig. 4*a*). ANA-C stained the interphase nuclei to produce an array of small dots consistent with centromeres/pre-kinetochores (Fig. 4*a*, *middle panel*). The GFP-hsMAD1 protein also presented constitutively in the interphase nuclei as bright *green*, slightly larger, nuclear punctates (Fig. 4*a*, *left*), some of which overlaid proximally with a subset of ANA-C stained dots (Fig. 4*a*, *right*).

The fact that GFP-hsMAD1 appeared constitutively in the nucleus prompted us to query as to how in human cells MAD1 might interact with MAD2. An initial report (27) on MAD2 had found it to be largely cytoplasmic in mammalian cells. In detergent fractionation of several types of human cells, we obtained results in agreement with this cytoplasmic predominance (data not shown). Because MSC checkpoint function obliges MAD2 to localize to kinetochores, one wonders whether this protein diffuses to kinetochores purely after mitotic dissolution of the nuclear envelope or whether some active fraction of human MAD2 might be in a centromere-proximal nuclear locale prior to mitosis. To address this question in the context of GFP-hsMAD1, we constructed a red fluorescent protein (RFP)-tagged hsMAD2 protein (Fig. 4*b*). Asynchronous HeLa cells were then transfected with GFP-hsMAD1-alone (Fig. 4*b*,

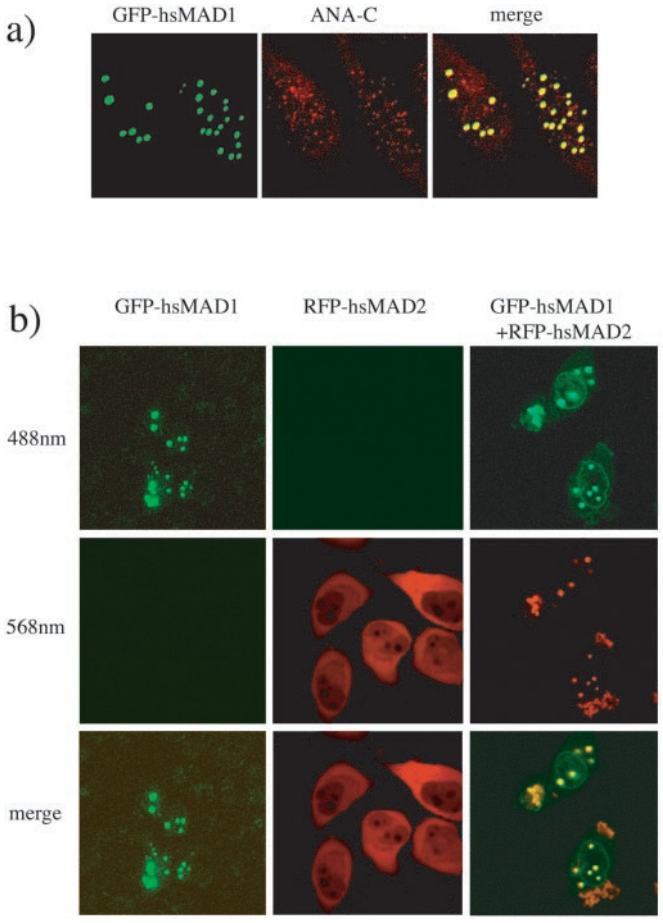

FIG. 4. **hsMAD1 congregates to nuclear punctates in interphase HeLa cells.** *a*, fluorescent visualization of GFP-tagged hsMAD1 (*green*) and ANA-C staining (*red*). Representative confocal microscopic images of methanol-fixed HeLa interphase cells transfected with GFP-tagged hsMAD1 and incubated with ANA-C serum which stains kinetochore precursors in interphase cells (see Ref. 54) are shown. A subset of *green* nuclear punctates are proximal to ANA-C staining. *b*, hsMAD1 relocates hsMAD2 into nuclear punctates. Confocal images of HeLa cells transfected with GFP-hsMAD1 alone (*left column*, *GFP-hsMAD1*), RFP-hsMAD2 alone (*middle column*, *RFP-hsMAD2*), or co-transfected with GFP-hsMAD1 + RFP-hsMAD2 (*right column*, *GFP-hsMAD1 + RFP-hsMAD2*). The 488-nm window visualizes GFP-tagged proteins; the 568-nm window visualizes RFP-tagged proteins.

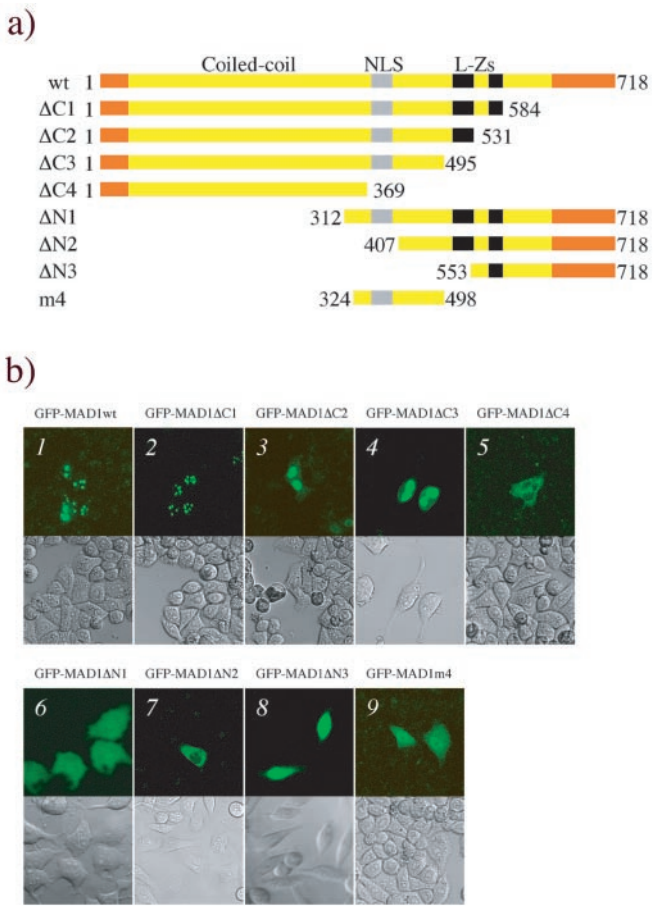

FIG. 5. **Regions of hsMAD1 required for localization into nuclear punctates.** *a*, schematic representations of wild type hsMAD1 and various deletion mutants of hsMAD1. Coiled-coil regions, nuclear localization signal (*NLS*), and two leucine zipper (*L-Zs*) domains were predicted using PSORT (psort.ims.u-tokyo.ac.jp) and are indicated in the schematic. *b*, *panels 1–9* show the subcellular localizations of GFP-tagged wild type hsMAD1 and seven deletion mutants. Confocal images are of HeLa cells transfected with the indicated GFP-tagged protein.

left column), RFP-hsMAD2-alone (Fig. 4*b*, *middle column*), or RFP-hsMAD2 + GFP-hsMAD1 together (Fig. 4*b, right column*). Green (488 nm) and red (568 nm) signals independently captured from the same cells permitted one to distinguish MAD1 from MAD2. GFP-MAD1-alone was found to be nuclear and in punctated configurations (Fig. 4*b*, *left column*); by contrast, RFP-hsMAD2-alone was faintly whole cell to largely cytoplasmic (Fig. 4*b*, *middle column*). This profile agrees with a previously mentioned whole cell pattern for GFP-yMAD2 in yeast (28) and suggests that in the pre-mitotic phase of the cell cycle MAD2 autonomously is incapable of specific nuclear localization. Interestingly, when GFP-MAD1 and RFP-MAD2 were simultaneously expressed in the same cell, RFP-MAD2 was quantitatively driven into GFP-MAD1 nuclear dots (Fig. 4*b, right column*). In these interphase cells, the GFP-hsMAD1 + RFP-hsMAD2-dots were indistinguishable from those of GFP-MAD1-alone (Fig. 3*b*, *left column*). This finding suggests that in human cells some portion of MAD2 can be actively localized into the nucleus by hsMAD1 prior to the dissolution of the nuclear envelope.

hsMAD1 is a 718-amino acid polypeptide with an extended coiled-coil (aa 48–631). It has a putative nuclear localization signal (aa 381–400) and two leucine zippers at aa 501–522 and aa 557–571 (Fig. 5*a*). We constructed eight deleted forms of GFP-hsMAD1 in order to further understand its determinants of subcellular localization (Fig. 5*a*). The eight GFP-hsMAD1 mutants included those progressively removed for C-terminal sequences (*i.e.* ΔC1–ΔC4), those progressively deleted for N-terminal sequences (*i.e.* ΔN1–ΔN3), and one containing the central 324–498 residues (m4). Each mutant was separately transfected into cells, and the cells were imaged by laser confocal microscopy. Among the eight forms of MAD1, only GFP-wild type MAD1 (Fig. 5*b*, *panel 1*) and GFP-MAD1ΔC1 (Fig. 5, *panel 2*) presented nuclear dots. GFP-MAD1ΔC2 and GFP-MAD1ΔC3, although not exhibiting a punctate pattern, appeared in the nucleus (Fig. 5*b*, *panels 3* and *4*). By contrast, GFP-MAD1ΔC4 and GFP-MAD1ΔN2 were nuclear-excluded (Fig. 5*b*, *panels 5* and *7*). Finally, GFP-MAD1ΔN1, GFP-MADΔN3, and GFP-MAD1m4 were found in both nucleus and cytoplasm (Fig. 5*b*, *panels 6*, *8*, and *9*). Collectively, these profiles suggest an intact leucine zipper at amino acids 557–571 (Fig. 5*a*) as being required for presentation of nuclear punctates and the 381–400 nuclear localization signal as being a necessary element for nuclear localization.

Leucine Zipper Domains in hsMAD1 Are Required for Intracellular Interaction with hsMAD2—To further detail human MAD1-MAD2 interactions, we next expressed RFP-hsMAD2 with various GFP-tagged hsMAD1 mutants (Fig. 5*a*). *En toto*,

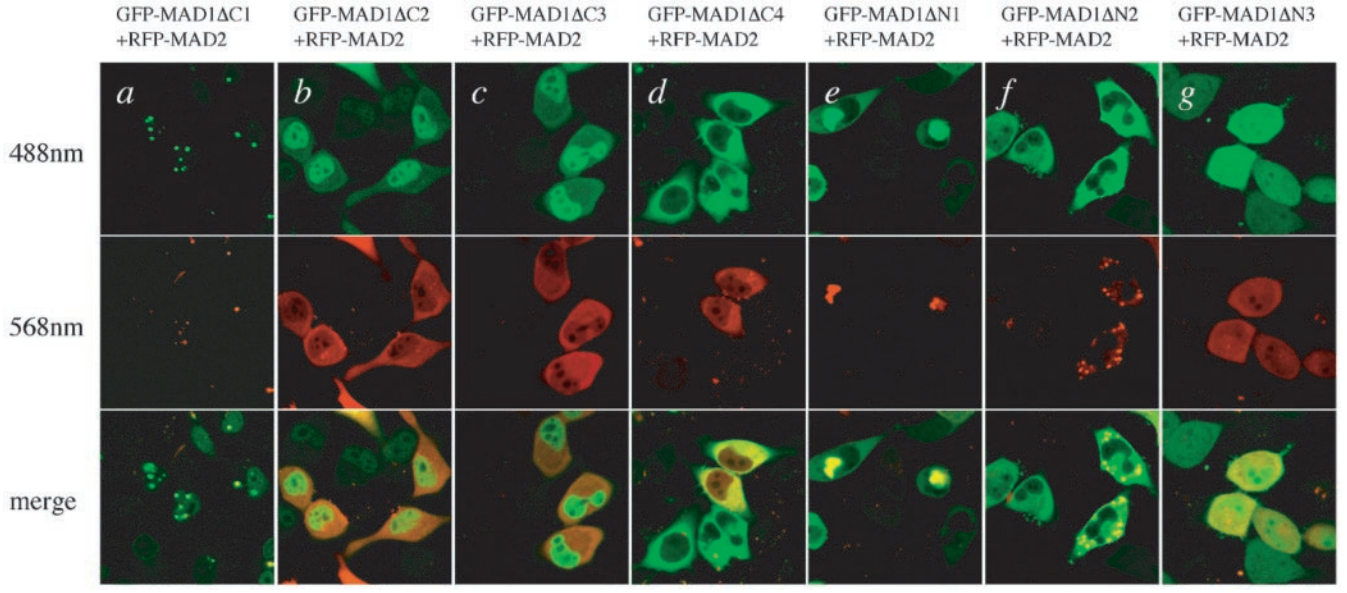

FIG. 6. **Domains in hsMAD1 that interact intracellularly with hsMAD2.** Various GFP-hsMAD1 mutant proteins were visualized in HeLa cells simultaneously with wild type RFP-hsMAD2. *Columns a–g*, confocal images of the indicated GFP-hsMAD1 mutant protein co-transfected with RFP-hsMAD2. *Top row* contains images captured at 488 nm; middle images are the same fields captured at 568 nm; *bottom panels* are merged images.

seven hsMAD1 mutants were analyzed (Fig. 6, *a–g*). Among the mutants, only GFP-hsMAD1ΔC1 (Fig. 6*a*) could relocalize RFP-hsMAD2 into nuclear dots. Interestingly, although neither GFP-hsMAD1ΔN1 (Fig. 6*e*) nor GFP-hsMAD1ΔN2 (Fig. 6*f*) produced nuclear punctates, both mutants did reorganize the stained morphology of RFP-hsMAD2. Thus these two MAD1 mutants, although aberrant unto themselves, appear to remain competent for intracellular contact with RFP-hsMAD2.

Based on the confocal images, we concluded that all MAD1 forms that affected MAD2 patterning (*e.g.* wild type GFP-hsMAD1, GFP-hsMAD1ΔC1, GFP-hsMAD1ΔN1, and GFP-hsMAD1ΔN2) maintained intact aa 501–522 and 557–571 leucine zippers. On the other hand, MAD1 forms that did not influence intracellular MAD2 staining (*e.g.* GFP-MAD1ΔC2; GFP-MAD1ΔC3, GFP-MAD1ΔC4, and GFP-MAD1ΔN3) were changed in either one or both zippers. To the extent that morphological changes in RFP-hsMAD2 occur via contact with GFP-hsMAD1, the profiles seen from GFP-hsMAD1ΔN1 (Fig. 6*e*) and GFP-hsMAD1ΔN2 (Fig. 7*f*) imply that both leucine zippers are necessary for intracellular MAD1-MAD2 binding. The confocal results describing MAD1-MAD2 contact are summarized in Table I.

The Entire hsMAD2 Is Needed to Interact Functionally with hsMAD1—We found previously that all hsMAD2 truncations abolished heterodimerization of MAD1-MAD2 *in vitro* (16). To compare *in vitro* results with intracellular MAD1-MAD2 interactions, we constructed wild type and four GFP-hsMAD2 truncation mutants (Fig. 7*a*). Each was tested for subcellular localization in the absence (Fig. 7*b, panels 1–5*) or presence (Fig. 7*b*, *panels 6–10*) of overexpressed untagged hsMAD1. GFP-hsMAD2 wild type (Fig. 7*b*, *panel 1*) produced green whole cell fluorescence that was dramatically converted to nuclear punctates by co-expressed hsMAD1 (Fig. 7*b*, *panel 6*). By contrast, all deletions in either N or C terminus destroyed the capacity of GFP-MAD2 to be efficiently reconfigured by hsMAD1 into nuclear dots (Fig. 7*b*, *panels 2–5* and *7–10*). Thus, consistent with our earlier *in vitro* binding results, intracellularly, the entire hsMAD2 protein is also required for efficient interaction with hsMAD1.

Loss of Heterozygosity at MAD1 Codon 558 in a Breast Cancer—The above results provide cell culture evidence that both

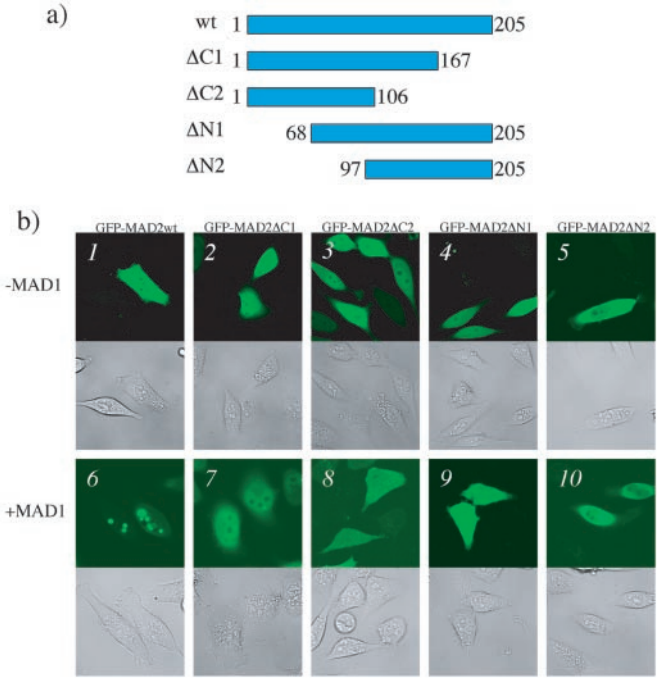

FIG. 7. **A requirement for intact hsMAD2 to interact with hsMAD1.** *a*, schematic representations of wild type hsMAD2 and four deletion mutants. *b*, *panels 1–10* contain representative confocal images of HeLa cells transfected with various GFP-hsMAD2 expression plasmids and co-transfected with either pUC19 (*panels 1–5*, *−MAD1*) or with wild type untagged hsMAD1 expression plasmid (*panels 6–10*, *+MAD1*).

leucine zipper domains in MAD1 are important for MAD1-MAD2 binding and that prior to the onset of mitosis MAD1 can convey MAD2 into nuclear punctates through direct contact. In the context of these observations, we note with interest that the MAD1H558 polymorphism impinges directly on the 557–571 leucine zipper needed for MAD1-MAD2 binding. To probe further the physiological significance of the MAD1R558/MAD1H558 polymorphism, we next sought *in vivo* evidence supportive of this change being advantageous for cellular pro-

TABLE I
Summary of hsMAD1 and hsMAD2 interactions based on confocal fluorescent images

MAD1	Localization	RFP-MAD2-relocalization[a]	MAD1/MAD2[b]
Wild-type (1–718)	Nuclear punctates	Nuclear punctates	+
ΔC1 (1–584)	Nuclear punctates	Nuclear punctates	+
ΔC2 (1–531)	Nucleus ≫ cytoplasm	Nucleus + cytoplasm	−
ΔC3 (1–495)	Nucleus ≫ cytoplasm	Nucleus + cytoplasm	−
ΔC4 (1–369)	Cytoplasm	Nucleus + cytoplasm	−
ΔN1 (312–718)	Nucleus + cytoplasm	Cytoplasm	+
ΔN2 (407–718)	Cytoplasm	Cytoplasm	+
ΔN3 (553–718)	Nucleus + cytoplasm	Nucleus + cytoplasm	−
m4 (324–498)	Nucleus + cytoplasm	Nucleus + cytoplasm	−
MAD2	**Localization**	**GFP-MAD2-relocalization[c]**	**MAD1/MAD2[b]**
Wild-type (1–205)	Nucleus+cytoplasm	Nucleus+ punctates	+
ΔC1 (1–167)	Nucleus+cytoplasm	Nucleus+cytoplasm	−
ΔC2 (1–106)	Nucleus+cytoplasm	Nucleus+cytoplasm	−
ΔN1 (68–205)	Nucleus+cytoplasm	Nucleus+cytoplasm	−
ΔN2 (97–205)	Nucleus+cytoplasm	Nucleus+cytoplasm	−

[a] RFP-tagged wild-type MAD2 in the presence of the indicated wild-type or mutant MAD1.
[b] MAD1/MAD2 interaction interpreted based on GFP or RFP relocalization results.
[c] Wild-type or mutant GFP-tagged MAD2 visualized in the presence of overexpressed wild-type MAD1.

liferation. A finding of loss of heterozygosity (LOH) at the *Mad1 558* locus would represent such *in vivo* evidence.

The *Acc*II restriction enzyme cleaves the "cgcg" sequence. In our search for LOH, we noted that the Arg to His single nucleotide polymorphism at codon 558 of hsMAD1 changes a "c**g**cg" to "c**a**cg," abolishing an *Acc*II site (Fig. 8*a*). Accordingly, *Acc*II restriction would be diagnostic for this 558 polymorphism. We analyzed the *Acc*II restriction of exon 17 from *hsMad1* in several human specimens; some illustrative results are shown in Fig. 8*b*. For instance, spindle checkpoint-defective SW480 colon cancer was homozygously *h*/*h* at position 558. On the other hand, the checkpoint intact Hct116 and HeLa cells (29) were *558r*/*r* and *558r*/*h*, respectively. To ask whether an Arg to His change could occur through somatic LOH, we examined eight breast tumor biopsies paired with their corresponding normal B cells. In one of eight (HCC1937) pairs, the heterozygous 558*r*/*h* genotype in the normal peripheral B cells was found to have converted to a homozygous 558*h*/*h* genotype in the matched breast tumor (Fig. 8*b, lanes 4* and *5*).

Expression of MAD1558H and Loss of Spindle Checkpoint in Colon Cancer Cells—The above results (Fig. 8) suggest that the *558h*/*h* genotype, at best, correlates with only a minority (*e.g.* 12.5%) of breast cancers. This could be consistent with the multifactorial basis for breast cancers in which important genetic components such as *BRCA1* and *BRCA2* account for between 1.5 and 2% of all breast tumors (30). Because we lacked detailed karyotypic information for the breast samples in Fig. 8, we turned to several well described colon cancer cells to further examine the correlation between *558r*/*r versus 558h*/*h* with aneuploidy and spindle checkpoint function (Fig. 9). In analyzing nine colon cancer cells, we found that five (SW480, SW48, LoVo, T84, and DLD-1) were *558h*/*h,* whereas two (SW837 and Hct116) were *558r*/*r*. Two others (Colo201 and HT29) were heterozygously *558r*/*h* (Fig. 9*A*).

Using the two homozygous colon cancer genotypes, we next asked how *558r*/*r* and *558h*/*h* might differ in spindle checkpoint function (Fig. 9*B*). When Hct116 (*558r*/*r*) was compared with SW480, SW48, LoVo, and T84 (*558h*/*h*) in mitotic arrest response to nocodazole, we found that the former cell was spindle checkpoint intact, whereas all of the latter cells were spindle checkpoint-defective (Fig. 9*B*). (DLD-1 and SW837 cells showed unexpectedly high levels of cell death in the presence of nocodazole, and mitotic indices were not assessed for these two cells.)

As an additional measure of the difference between MAD1 558R and MAD1 558H, we assessed spindle checkpoint function when the two different MAD1 proteins were introduced into a cell with homogeneous *558h*/*h* background. Thus, we transfected SW480 cells to overexpress either MAD1 558H or 558R. In transfected cell cultures, we consistently observed

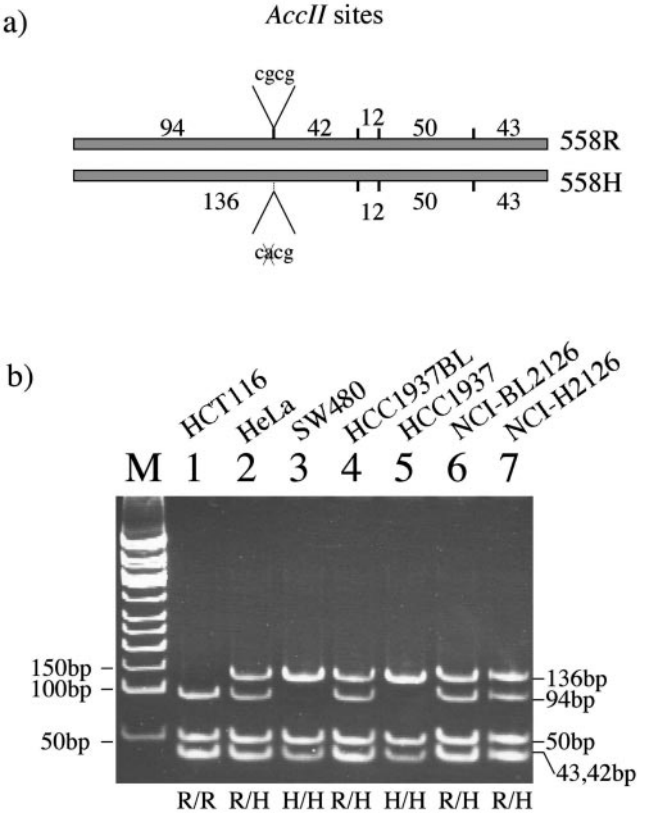

FIG. 8. **Detection of somatic loss of Arg-558/His-558 (*558R/558H*) heterozygosity in a breast cancer.** *a*, schematic representation of *Acc*II restriction sites within a genomic PCR-amplified fragment from exon 17 of *hsmad1*. *Acc*II cleaves the Arg-558 (*558R*) allele to yield fragments of 94, 50, 43, 42, and 12 bp and cleaves the His-558 (*558H*) allele to fragments of 136, 50, 43, and 12 bp. *b*, *Acc*II restriction patterns resolved by electrophoresis in 12% polyacrylamide gel of PCR-amplified genomic DNA. HCC1937, a breast cancer cell line with aneuploidy, shows homozygosity for the His-558 polymorphism (*lane 5*), whereas HCC1937BL, the Epstein-Barr virus-transformed normal B-lymphoblastoid cell line from the same individual, is heterozygously Arg-558/His-558 (*lane 4*). Another breast cancer/normal matched pair showed no change between tumor and normal tissue (*lanes 6* and *7*). Restriction patterns for HeLa, Hct116, and SW480 cell lines are also presented.

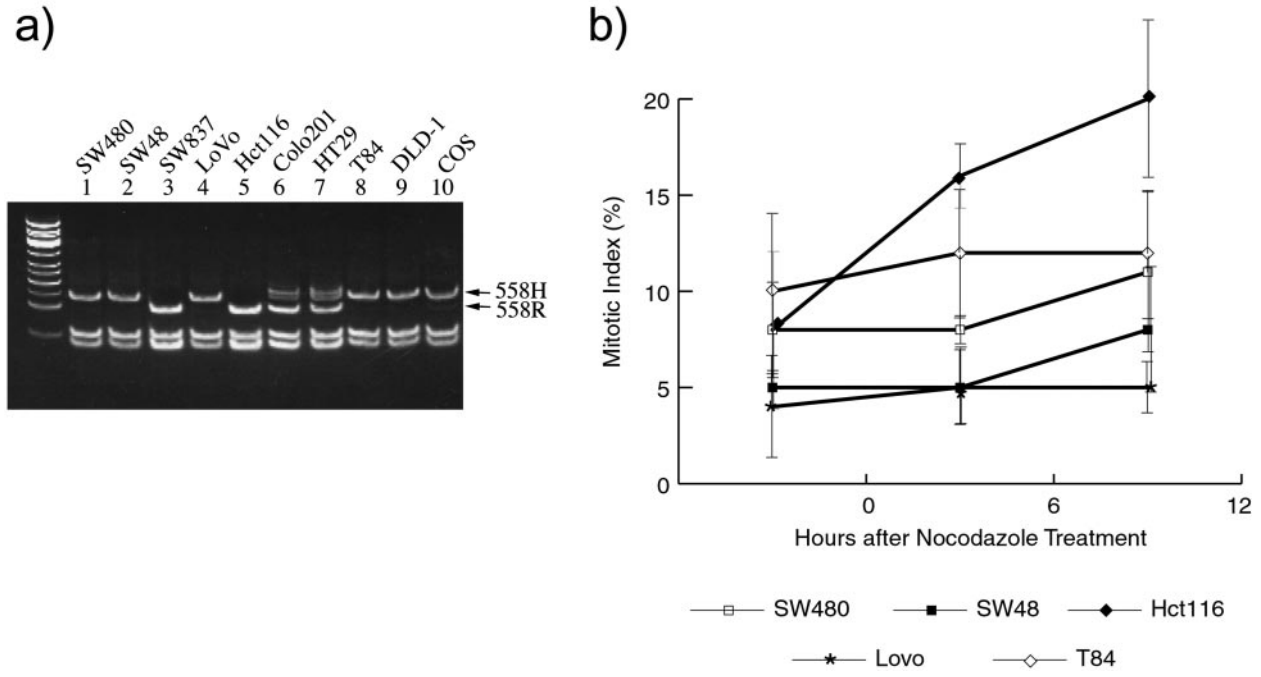

FIG. 9. **Characterization of MAD1 polymorphism in nine colon cancer cells.** *a*, analyses of the genotype at position 558 of *hsMad1* in nine colon cancer cells (*lanes 1–9*). COS cell (*lane 10*) is an African green monkey kidney cell transformed by SV40. Analyses were performed as described in Fig. 8. *b*, mitotic index comparisons between Hct116 (*558r/r*) and four *558h/h* colon cancers (SW48, SW480, Lovo, and T84). The former genotype exhibits mitotic arrest in response to nocodazole, whereas the latter genotype shows a defect in arrest function. Results are average values from three independent assays. Hct116 is diploid, and SW48, SW480, LoVo, and T84 are aneuploid.

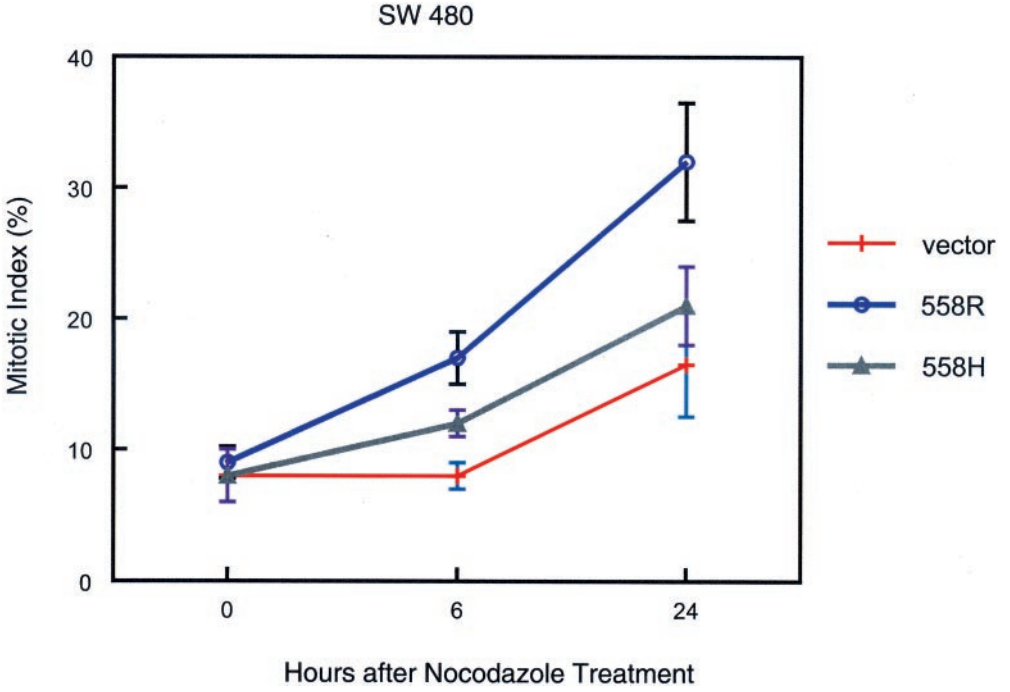

FIG. 10. **Expression of MAD1R558 enhances nocodazole-induced mitotic arrest in SW480 cells.** Mitotic index analyses were performed as described in Fig. 2. Results shown are average values from three independent assays.

that overexpressed MAD1 558R rescued the otherwise defective spindle checkpoint response of SW480 cells to nocodazole (Fig. 10).

DISCUSSION

Perturbation in several discrete pathways can lead to aneuploidy in mammalian cells (31–34). One of several gatekeepers of euploidy is the mitotic spindle assembly checkpoint (MSC). Among the many components of the spindle checkpoint, studies in yeast and mammals have identified MAD2 as the key downstream effector in the metaphase-to-anaphase censor against chromosomal missegregation during mitosis (9, 28, 35–37). Considering that spindle checkpoint loss can contribute to aneuploidy and that 70–80% of all cancer cells are aneuploid, one reasonably expects to find frequent *Mad2* (and perhaps other checkpoint components) mutations in human malignancies. Curiously, intensive targeted searches for mutations in the spindle checkpoint genes have revealed such to be exceedingly

rare in human tumors (11, 38–41). Hence, an unanswered cancer paradox is how to reconcile frequent checkpoint loss with rarity of checkpoint gene mutations.

HsMAD1 is the intracellular binding partner for hsMAD2 (16). Thus, loss of hsMAD2 function could emanate from changes in hsMAD1. Here we have characterized the domains in hsMAD1 needed to interact with hsMAD2. We found that two leucine zipper domains (amino acids 501–522 and 557–571) are required for hsMAD1 to bind hsMAD2. In several cancer cells, a coding single nucleotide Arg to His polymorphism at codon 558, which disrupts the second leucine zipper of hsMAD1, was frequently observed. This R558H change in hsMAD1 was seen in over 50% of our surveyed human cancers (Fig. 1), including 7 of 9 colon cancers (Fig. 9*A*). One of eight breast cancer samples examined by us also showed evidence for LOH at codon 558 of hsMAD1 (Fig. 8). Interestingly, when we surveyed anonymous peripheral blood samples from 14 normal individuals, 6 were heterozygously *558h/r*; 8 were homozygously *558r/r*; none were homozygously *558h/h* (data not shown). Thus, whereas larger surveys are needed to determine the extent of *558h* in the gene pool and the potential frequency of LOH in cancers, the extant data do support that 558H is a common human MAD1 polymorphism. If the properties of 558H as described here are correct, our findings could imply that a genotypic proclivity for loss of spindle checkpoint function may be more common than conventionally anticipated.

Our study comments on two mechanistic issues regarding MSC function in human, *Xenopus*, and yeast. Studies on Xmad1 and Xmad2 in soluble meiotic extracts have shown that Xmad1 dominantly locates Xmad2 to kinetochores (23, 28). Here we observed that in interphase human cells, hsMAD1 dominantly directs hsMAD2 into nuclear punctate bodies; some of these bodies appear to overlap with ANA-C staining. If one analogizes the human findings to the Xmad1/Xmad2 model, a reasonable interpretation, which does not necessarily exclude others, is that during interphase human MAD1 directs nuclear migration of a subset of MAD2 to centromere-proximal (42) nuclear locales. These hsMAD1-hsMAD2 complexes could thus be poised for checkpoint function in the ensuing mitotic phase of the cell cycle. It is likely that further protein-protein interactions are required to trigger hsMAD1/hsMAD2 checkpoint activity. In this regard, it has been reported that the CENP-E protein, which is synthesized subsequent to interphase (43), is needed for Xmad1/Xmad2 to bind kinetochores in meiotic extracts (24). Intriguingly, in mitotic HeLa cells, MAD2 was found to bind kinetochores despite deliberate depletion of CENP-E (25). Although our current data do not permit us to distinguish between these two competing views, we note that Mad1/Mad2 function in yeast is apparently CENP-E-independent because no CENP-E-like protein exists in the yeast genome (24).

Our characterization of hsMAD1 behavior in cancer cells adds insight to existing studies on hsMAD2 and hsBUB1 and provides an initial platform for addressing the relative interplay between these checkpoint components. The findings here are consistent with the polymorphic MAD1H558 protein being less capable than MAD1R558 in binding hsMAD2 and in enforcing spindle assembly checkpoint function in cultured cells. These results clarify for the first time that two intact leucine zipper domains in hsMAD1 are mechanistically required for binding hsMAD2, and they extend further support to the notion that binding by hsMAD1 is important for hsMAD2 function. Despite the suggestive findings from cultured cells, a conclusive deduction that the His-558 polymorphism affects *in vivo* spindle checkpoint function awaits epidemiological case control studies. Additional work is also needed to fully address the relationship of loss of spindle checkpoint function with the development of aneuploidy *in vivo*.

Acknowledgments—We thank Warren Leonard and Christine Kozak for critical readings of manuscript, George Dapolito for technical assistance, and Lan Lin for preparation of manuscript.

REFERENCES

1. Amon, A. (1999) *Curr. Opin. Genet. Dev.* **9,** 69–75
2. Wassmann, K., and Benezra, R. (2001) *Curr. Opin. Genet. Dev.* **11,** 83–90
3. Heim, S., and Mitelman, F. (1995) *Cancer Cytogenesis,* 2nd Ed., pp. 1–17, Wiley-Liss, Inc., New York
4. Li, R., and Murray, A. W. (1991) *Cell* **66,** 519–531
5. Hoyt, M. A., Totis, L., and Roberts, B. T. (1991) *Cell* **66,** 507–517
6. Abrieu, A., Magnaghi-Jaulin, L., Kahana, J. A., Peter, M., Castro, A., Vigneron, S., Lorca, T., Cleveland, D. W., and Labbe, J. C. (2001) *Cell* **106,** 83–93
7. Fisk, H. A., and Winey, M. (2001) *Cell* **106,** 95–104
8. Li, Y., Gorbea, C., Mahaffey, D., Rechsteiner, M., and Benezra, R. (1997) *Proc. Natl. Acad. Sci. U. S. A.* **94,** 12431–12436
9. Elledge, S. J. (1998) *Science* **279,** 999–1000
10. Wassmann, K., and Benezra, R. (1998) *Proc. Natl. Acad. Sci. U. S. A.*, **95,** 11193–11198
11. Tighe, A. Johnson, V. L. Albertella, M., and Taylor, S. S. (2001) *EMBO Rep.* **2,** 609–614
12. Takahashi, T., Haruki, N., Nomoto, S., Masuda, A., Saji, S., Osada, H., and Takahashi, T. (1999) *Oncogene* **18,** 4295–4300
13. Cahill, D. P., Lengauer, C., Yu, J., Riggins, G. J., Willson, J. K. V., Markowitz, S. D., Kinzler, K. W., and Vogelstein, B. (1998) *Nature* **392,** 300–303
14. Shah, J. V., and Cleveland, D. W. (2000) *Cell* **103,** 997–1000
15. Howell, B. J., Hoffman, D. B., Fang, G., Murray, A. W., and Salmon, E. D. (2000) *J. Cell Biol.* **150,** 1233–1249
16. Jin, D. Y., Spencer, F., and Jeang, K. T. (1998) *Cell* **93,** 81–91
17. Sironi, L., Melixetian, M., Faretta, M., Prosperini, E., Helin, K., and Musacchio, A. (2001) *EMBO J.* **20,** 6371–6382
18. Cahill, D. P., da Costa, L. T., Carson-Walter, E. B., Kinzler, K. W., Vogelstein, B., and Lengauer, C. (1999) *Genomics* **58,** 181–187
19. Percy, M. J., Myrie, K. A., Neeley, C. K., Azim, J. N., Ethier, S. P., and Petty, E. M. (2000) *Genes Chromosomes Cancer* **29,** 356–362
20. Chun, A. C., Zhou, Y., Wong, C. M., Kung, H. F., Jeang, K. T., and Jin, D. Y. (2000) *AIDS Res. Hum. Retroviruses* **16,** 1689–1694
21. Meek, D. W. (2000) *Pathol. Biol.* (*Paris*) **48,** 246–254
22. Jin, D. Y., Kozak, C. A., Pangilinan, F., Spencer, F., Green, E. D., and Jeang, K. T. (1999) *Genomics* **55,** 363–364
23. Chen, R. H., Shevchenko, A., Mann, M., and Murray, A. W. (1998) *J. Cell Biol.* **143,** 283–295
24. Abrieu, A., Kahana, J. A., Wood, K. W., and Cleveland, D. W. (2000) *Cell* **102,** 817–826
25. Yao, X., Abrieu, A., Zheng, Y., Sullivan, K. F., and Cleveland, D. W. (2000) *Nature Cell Biol.* **2,** 484–491
26. Campbell, M. S., Chan, G. K., and Yen, T. J. (2000) *J. Cell Sci.* **114,** 953–963
27. O'Neill, T. J., Zhu, Y., and Gustafson, T. A. (1997) *J. Biol. Chem.* **272,** 10035–10040
28. Chen, R. H., Brady, D. M., Smith, D., Murray, A. W., and Hardwick, K. G. (1999) *Mol. Biol. Cell* **10,** 2607–2618
29. Bunz, F., Dutriaux, A., Lengauer, C., Waldman, T., Zhou, S., Brown, J. P., Sedivy, J. M., Kinzler, K. W., and Vogelstein, B. (1998) *Science* **282,** 1497–1501
30. Venkitaraman, A. R. (2002) *Cell* **108,** 171–182
31. Sen, S. (2000) *Curr. Opin. Oncol.* **12,** 82–88
32. Duensing, S., and Munger, K. (2001) *Biochim. Biophys. Acta* **1471,** M81–88
33. Fodde, R., Kuipers, J., Rosenberg, C., Smits, R., Kielman, M., Gaspar, C., van Es, J. H., Breukel, C., Wiegant, J., Giles, R. H., and Clevers, H. (2001) *Nature Cell Biol.* **4,** 433–438
34. Livingston, D. M. (2001) *Nature* **410,** 536–537
35. Li, Y., and Benezra, R. (1996) *Science* **274,** 246–248
36. Fang, G., Yu, H., and Kirschner, M. W. (1998) *Genes Dev.* **12,** 1871–1883
37. Dobles, M., Liberal, V., Scott, M. L., Benezra, R., and Sorger, P. K. (2000) *Cell* **101,** 635–645
38. Imai, Y., Shiratori, Y., Kato, N., Inoue, T., and Omata, M. (1999) *Jpn. J. Cancer Res.* **90,** 837–840
39. Yamaguchi, K., Okami, K., Hibi, K., Wehage, S. L., Jen, J., and Sidransky, D. (1999) *Cancer Lett.* **139,** 183–187
40. Sato, M., Sekido, Y., Horio, Y., Takahashi, M., Saito, H., Minna, J. D., Shimokata, K., and Hasegawa, Y. (2000) *Jpn. J. Cancer Res.* **91**, 504–509.
41. Myrie, K. A., Percy, M. J., Azim, J. N., Neeley, C. K., and Peety, E. M. (2000) *Cancer Lett.* **152**, 193–199.
42. Alberts, B., Bray, D., Lewis, J., Raff, M., Roberts, K., and Watson, J. D. (1994) *Molecular Biology of the Cell,* 3rd Ed., pp. 335–400, Garland Publishing Inc., New York
43. Jablonski, S. A., Chan, G. K., Cooke, C. A., Earnshaw, W. C., and Yen, T. J. (1998) *Chromosoma* **107,** 386–396